Version: 11.12.2020

# New Tools to Probe the Protein Surface: Ultrasmall Gold Nanoparticles Carry Amino Acid Binders

Selina Beatrice van der Meer,[1] Inesa Hadrovic,[2] Annika Meiners,[3] Kateryna Loza,[1] Marc Heggen,[4] Shirley K. Knauer,[3] Peter Bayer,[5] Thomas Schrader,[2] Christine Beuck,[5,*] and Matthias Epple[1,*]

[1] Inorganic Chemistry and Center for Nanointegration Duisburg-Essen (CeNIDE), University of Duisburg-Essen, Universitätsstr. 5-7, 45117 Essen, Germany

[2] Organic Chemistry, University of Duisburg-Essen, Universitätsstr. 5-7, 45117 Essen, Germany

[3] Department of Molecular Biology II, Centre Centre for Medical Biotechnology (ZMB), University of Duisburg-Essen, Essen, Germany

[4] Ernst Ruska-Centre for Microscopy and Spectroscopy with Electrons, Forschungszentrum Jülich GmbH, 52425 Jülich, Germany

[5] Department of Structural and Medicinal Biochemistry, Centre for Medical Biotechnology (ZMB), University of Duisburg-Essen, Essen, Germany

* Corresponding authors;
e-mails christine.beuck@uni-due.de and matthias.epple@uni-due.de

**Abstract**

A strategy towards epitope-selective functionalized nanoparticles is introduced: Ultrasmall gold nanoparticles (diameter of the metallic core about 2 nm) were functionalized with molecular tweezers that selectively address lysine and arginine residues on protein surfaces. Between 11 and 30 tweezer molecules were covalently attached to the surface of each nanoparticle by copper-catalyzed azide alkyne cycloaddition (CuAAC), giving multiavid agents to target proteins. The nanoparticles were characterized by high-resolution transmission electron microscopy (HRTEM), differential centrifugal sedimentation (DCS), and $^{1}$H-NMR spectroscopy (diffusion-ordered spectroscopy DOSY, and surface composition). The interaction of these nanoparticles with the model proteins hPin1 (WW domain; hPin1-WW) and Survivin was probed by NMR titration and by isothermal titration calorimetry (ITC). The binding to the WW domain of hPin1 occurred with a $K_D$ of 41 ± 2 μM as shown by ITC. The nanoparticle-conjugated tweezers targeted cationic amino acids on the surface of hPin1-WW in the following order: N-terminus (G) ≈ R17 > R14 ≈ R21 > K13 > R36 > K6 as shown by NMR spectroscopy. Nanoparticle recognition of the larger protein Survivin was even more efficient and occurred with a $K_D$ of 8 ± 1 μM as shown by ITC. We conclude that ultrasmall nanoparticles can act as versatile carriers for artificial protein ligands and strengthen their interaction with the complementary patches on the protein surface.

**Keywords:** Gold, nanoparticles, molecular tweezers, proteins, supramolecular chemistry

## Introduction

The selective targeting of protein epitopes is a promising way to influence a protein's function. This is frequently used in pharmaceutic chemistry to inhibit or activate proteins, typically by small molecules ("ligands") where concepts from supramolecular chemistry have been applied as well.[1-5] Extending the field beyond molecules, nanoparticles have been proposed as selective binders for proteins, e.g. for enzyme inhibition by binding to the active center.[6-12] This is especially interesting when ultrasmall nanoparticles (1-2 nm diameter) are used which are small in comparison to proteins and meet the dimension of metal clusters.[6, 10, 13, 14] They are also able to enter cells[13, 15-17] and in some cases also the cell nucleus.[14, 18, 19] However, a viable strategy for a covalent attachment of selective supramolecular ligands to ultrasmall nanoparticles is still missing. Such a strategy would lead to multiavid nanoparticles with an increased protein binding affinity.

Specific targeting ligands can be covalently attached via copper-catalyzed azide-alkyne cycloaddition (CuAAC; a "click reaction") to the surface of gold nanoparticles.[20-32] If the nanoparticle is ultrasmall, its surface composition can be directly probed by solution NMR spectroscopy, giving both the amount and the chemical nature of the attached receptor molecules, an approach that is unfeasible for larger nanoparticles.[32-37] This surface functionalization allows a specific interaction between the immobilized ligands and the target protein.[6] The high local concentration of the ligand molecules can then lead to an increased avidity that we denote as multiavidity in the following.[6, 32] Entropically, this leads to a higher probability to target a given protein epitope.

Molecular tweezers developed by Klärner and Schrader have turned out to be selective and efficient binders for cationic amino acids, especially when exposed on the surface of proteins.[38-40] They are based on a specific three-dimensional structure

where a defined cavity is formed by alternating units of benzene and norbornadiene. This forms a rigid host molecule with a negatively polarized cavity that can accommodate a guest molecule with aliphatic chains and cationic end groups. The positively charged group of a guest molecule is able enter the cavity of the tweezer and interact with the phosphate anion at the central benzene unit. As a result, these molecular tweezers selectively bind to the side chains of lysine (K) and arginine (R) in amino acids, peptides, and proteins. Importantly, only the sterically accessible arginines and lysines of a protein are addressed.[41, 42]

Here we demonstrate how the surface of ultrasmall gold nanoparticles can be covalently functionalized with molecular tweezers as selective ligands for different protein surfaces. The interaction of such multiavid agents with the model proteins hPin1 (WW domain)[43-47] and Survivin.[48-51] is then quantitatively monitored on the molecular scale by NMR spectroscopy and isothermal titration calorimetry (ITC).

## Methods

### *Chemicals*

A solution of tetrachloroauric acid ($HAuCl_4$) was prepared by dissolving elemental gold (≥ 99%) in *aqua regia*. Sodium borohydride ($NaBH_4$, ≥ 96%), (+)sodium L-ascorbate (≥ 99%), copper(II)sulphate pentahydrate (≥ 99%), tris(3-hydroxypropyl-triazolylmethyl)amine (THPTA, ≥ 95%), and deuterium oxide ($D_2O$, 99%) were obtained from Sigma-Aldrich. Dipotassium hydrogenphosphate (p.a.) and potassium dihydrogen phosphate (p.a.) were obtained from Panreac Applichem. Aminoguanidine hydrogen carbonate (≥ 98%) was obtained from Alfa Aesar. The tripeptide 6-azido-lysine-cysteine-asparagine K($N_3$)CD (≥ 95%) was obtained from EMC Microcollections (Tübingen, Germany). Ultrapure water (Purelab ultra instrument from ELGA) was used for all syntheses and purifications unless otherwise

noted. For all reactions involving nanoparticles, all glassware was cleaned with boiling *aqua regia* and thoroughly washed with water afterwards.

***Synthesis***

The ultrasmall gold nanoparticles were prepared by a modified one-phase Brust synthesis.[32, 52] The cysteine- and azide-containing peptide K($N_3$)CD (4.5 µmol) was dissolved in 6 mL water. The pH was adjusted to 7 by addition of 0.1 M sodium hydroxide solution under continuous stirring. The solution was degassed with argon, and 30 µL of 50 mM tetrachloroauric acid (1.5 µmol) were added. After the yellow color of tetrachloroauric acid had vanished, 22.5 µL of a 200 mM ice-cold aqueous sodium borohydride solution (4.5 µmol) were added. After the addition of sodium borohydride, the solution rapidly turned brown, and the dispersion was stirred for one more hour at room temperature. The nanoparticle dispersion was passed through an ultrafiltration spin column (3 kDa molecular weight cut-off; Amicon®; Merck) for 20 min at 14,000 g to remove all unreacted compounds. The nanoparticles remained on the filter. After centrifugation, the filter was rinsed three times with potassium phosphate buffer (pH 8). By reverse centrifugation, the concentrated gold nanoparticles (~70 µL) with the K($N_3$)CD ligand covalently attached via the thiol group of cysteine.[53] were recovered from the filter. Alkyne-functionalized tweezer molecules were conjugated to the azide-terminated gold nanoparticles by copper-catalyzed azide-alkyne cycloaddition (CuAAC) in analogy to the coupling of alkyne-functionalized dyes.[32] The tweezer-conjugated nanoparticles were thoroughly purified by ultrafiltration and reverse centrifugation in the same way as described above. Special care was given to remove any unbound tweezer.

A monophosphate monobutynylphosphate tweezer was obtained in a 17-step total synthesis developed for unsymmetric diphosphate monoesters as described by Heid

et al.[40] The trichloroacetonitrile route was followed for the functionalization of the parent molecular tweezer with the clickable ester alcohol moiety. Figure 1 shows the basic reaction steps and the analytical characterization data.[40]

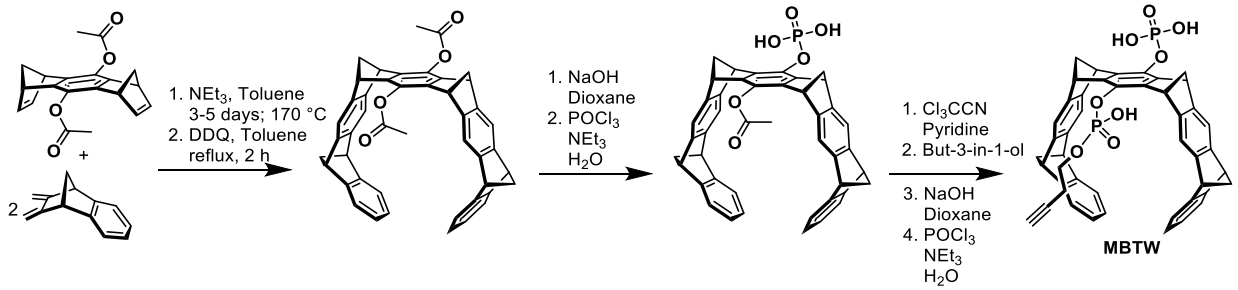


**Figure 1:** Synthesis of the monophosphate monobutynylphosphate tweezer (MBTW).[40]

The concentration of the nanoparticle-conjugated tweezer molecules was determined by ultraviolet-visible (UV-VIS) spectroscopy with unbound tweezer as calibration standard. For quantification of the clicked amount of tweezers, the aromatic absorption band of 260-310 nm from a dilution series of pure tweezers was integrated and plotted against the concentration. From the slope of the linear regression, the tweezer concentration was determined according to Lambert-Beer's law. The number of tweezers attached to each nanoparticle varied between the synthetic batches and was therefore separately determined for each batch.

***Protein expression and purification***

The hPin1-WW domain (residues 3-39; hPin1-WW) was expressed as N-terminal GST fusion protein with a PreScission protease cleavage site and purified as described earlier.[54] The $^{13}C$,$^{15}N$- or $^{15}N$-labeled protein for NMR titrations was expressed in *E. coli* BL21 (DE3) T1r in M9 minimal medium containing $^{15}NH_4Cl$

and $^{13}C$- or $^{12}C$-glucose, while unlabeled protein for ITC experiments was expressed in LB medium. The protein was purified by GSH affinity chromatography, followed by cleavage of the GST tag with a PreScission protease and subsequent size exclusion chromatography. Protein NMR samples contained 300 µM of the $^{13}C$,$^{15}N$-labeled protein or 50 µM of the $^{15}N$-labeled protein in 50 mM KPi (pH 8.0) with 10% $D_2O$.

GST-tagged truncated Survivin (amino acids 1-120) was expressed in *E. coli* SoluBL21 in 2 L LB medium supplemented with 25 µg $mL^{-1}$ kanamycin.[1] Bacteria were grown at 37 °C. Protein expression was induced with 0.2 mM IPTG at an $OD_{600}$ of 1.0 to 1.2 over 20 h at 30 °C. Cells were pelleted and lysed by sonication in PBS (pH 7.4) supplemented with 1 mM PMSF and 50 µg $mL^{-1}$ Lysozyme. GST-Survivin was purified with a GSTrap 4B affinity column, and the tag was cleaved by PreScission protease for 8 h at 4 °C. Subsequent size exclusion chromatography was performed with a HiLoad 26/600 Superdex 75 pg column and a GSTrap 4B column mounted beneath in 50 mM KPi pH 7.4 with 150 mM KCl and 2 mM DTT. Survivin was concentrated and dialyzed against PBS buffer with 10 kDa MWCO dialysis units.

***Nanoparticle characterization***

The concentrations of gold and copper in the nanoparticle dispersion were determined by atomic absorption spectroscopy (AAS) with a Thermo Electron M-Series spectrometer (graphite tube furnace according to DIN EN ISO/IEC 17025:2005) after dissolving the nanoparticles in *aqua regia*. Analytical disc centrifugation (differential centrifugal sedimentation; DCS) was performed with a CPS Instruments DC 24000 disc centrifuge (24,000 rpm). Two sucrose solutions (8 wt% and 24 wt%) formed a density gradient that was capped with 0.5 mL

dodecane as stabilizing agent. The calibration standard was a poly(vinyl chloride) (PVC) latex in water with a particle size of 483 nm provided by CPS Instruments. This calibration was carried out before each run. A sample volume of 100 µL of dispersed nanoparticles was used. The recording time was about 6 h at the given centrifugation speed. The density of elemental gold (19,300 kg $m^{-3}$) was used for the computations. UV-VIS spectroscopy was performed with a Varian Cary 300 instrument from 200 to 800 nm after background solvent correction (water). Suprasil® quartz glass cuvettes with a sample volume of 600 µL were used. High-resolution transmission electron microscopy was performed with an aberration-corrected FEI Titan transmission electron microscope equipped with a Cs-probe corrector (CEOS Company) operated at 300 kV.[55]

***NMR spectroscopy***

The nanoparticle samples were dispersed in 600 µL $D_2O$ for NMR spectroscopy. $^1$H-NMR spectra were recorded with a Bruker Avance III 600 MHz spectrometer at room temperature. $^1$H-DOSY experiments (diffusion-ordered spectroscopy) were performed at 25 °C on a Bruker Avance III 700 MHz spectrometer equipped with a 5 mm TCI $^1$H/$^{13}$C/$^{15}$N/D cryoprobe with a z-gradient in non-spinning mode using a 3 mm NMR tube. A presaturation pulse was added to the $^1$H-DOSY pulse sequence from the Bruker library to suppress the remaining water signal. The diffusion time was set to $\Delta$ = 100 ms and the pulsed gradient duration to $\delta$ = 4 ms for tweezer-functionalized ultrasmall gold nanoparticles. The diffusion time was set to $\Delta$ = 100 ms and the pulsed gradient duration to $\delta$ = 2.5 ms for dissolved tweezer molecules. The gradient strength was incremented in 32 steps from 5 to 95% of the maximum gradient strength (50.4 G $cm^{-1}$ for a smoothed square gradient pulse) with a linear ramp. The spectra were Fourier-transformed, phased and integrated using

Topspin 3.5. Plotting and fitting of the linearized diffusion data according to the Stejskal-Tanner equation[56, 57] were performed with Origin Pro 2017:

$$\ln\left(\frac{I}{I_0}\right) = -\gamma^2\delta^2\left(\Delta - \delta/3\right)\cdot D\cdot G^2 \quad (1)$$

with $I$ the signal intensity, $I_0$ the signal intensity without gradient, $\gamma$ the gyromagnetic ratio of $^1$H, $\delta$ the diffusion gradient pulse length, $\Delta$ the diffusion delay, $G$ the gradient strength, and $D$ the translational diffusion coefficient.

The Stejskal-Tanner plots of all nanoparticle signals were first analyzed separately. If the same diffusion coefficient, within the error margin, was obtained for all signals, the relative intensities $I/I_0$ were averaged. Error bars of the averaged data points represent the standard deviation of this computation.

The hydrodynamic diameter of the functionalized nanoparticle was then calculated by the Stokes-Einstein equation:

$$d_H = \frac{\mathrm{k}\cdot T}{3\pi\cdot\eta\cdot D} \quad (2)$$

with $d_H$ the hydrodynamic diameter, k the Boltzmann constant, $T$ the temperature in K, $\eta$ the dynamic viscosity of $D_2O$ at 25 °C, and $D$ the translational diffusion coefficient.

The binding of the tweezer-functionalized nanoparticles to $^{13}$C,$^{15}$N-lysine or hPin1-WW ($^{13}$C,$^{15}$N- or $^{15}$N-labeled) was assessed by NMR titrations in a 3 mm NMR tube on a Bruker Avance III 700 MHz spectrometer with a 5 mm TCI cryoprobe. Tweezer-functionalized nanoparticles were added stepwise to 300 µM $^{13}$C,$^{15}$N-lysine or $^{13}$C,$^{15}$N-labeled hPin1-WW, and lysine- and arginine-specific H2(C)N

experiments[54, 58-60] were recorded for each titration step. Relative signal intensities $I/I_0$ were corrected for the dilution of the sample after nanoparticle addition, plotted against the nanoparticle concentration, and fitted with an exponential decay function to assess the rate of signal decay.[54]

Furthermore, $^{15}$N-HSQC titration experiments of tweezer-functionalized nanoparticles or free monobutynyl tweezer molecules to 50 µM $^{15}$N-labeled hPin1-WW were performed. The chemical shift perturbations $\Delta\delta_{total}$ of the free tweezer were calculated from the $^{1}$H and $^{15}$N chemical shift differences ($\Delta\delta_H$ and $\Delta\delta_N$) as follows:[61]

$$\Delta\delta_{total} = \sqrt{\left(\Delta\delta_H\right)^2 + \left(0.154 \cdot \Delta\delta_N\right)^2} \quad (3)$$

For the nanoparticles, chemical shift perturbation analysis was not possible because the signals of residues involved in binding experienced strong line broadening and disappeared at low ligand concentrations which made it impossible to track their positions. Instead, relative signal intensities (corrected for the dilution) were plotted against the ligand concentration, and the curves were fitted as described for the H2(C)N signal intensities. The signal decay rates of the H2(C)N and HSQC experiments served to qualitatively assess the order of ligand binding but are not directly comparable between the two different experiments because the line broadening also depends on the relaxation rates of the involved nuclei.

***Isothermal titration calorimetry (ITC)***

ITC was performed with a MicroCal iTC200 from Malvern Panalytical at 25 °C with tweezers (control) or nanoparticles in the cell and proteins in the syringe. The proteins were dialyzed overnight at 4 °C against the corresponding buffer using dialysis units with 3 kDa MWCO for hPin1-WW and 10 kDa MWCO for Survivin.

ITC titrations with hPin1-WW were performed in 50 mM KPi/90 mM KCl at pH 8.0. Experiments with Survivin were performed in PBS at pH 7.4. Nanoparticles were dissolved in the corresponding dialysis buffer. ~150 μM tweezer molecules attached to gold nanoparticles ($c$(Au) = 250 μg $mL^{-1}$) were titrated with a 3.5 mM solution of hPin1-WW. ~30 μM tweezer molecules attached to gold nanoparticles ($c$(Au) = 170 μg $mL^{-1}$) were titrated with a 1.2 mM solution of Survivin. As control, azide-terminated nanoparticles ($c$(Au) = 170 μg $mL^{-1}$) were titrated with the proteins at the given concentrations. The cell was filled with 275 μL. 38 injections (1 μL each) were added with an equilibration time of 120 to 150 s between the injections. The injection rate was 2 μL $s^{-1}$. The reference power was 5 μcal $s^{-1}$. ITC thermograms were fitted with a stoichiometric equilibrium approach with the software AFFINImeter.

**Results and discussion**

Azide-terminated ultrasmall gold nanoparticles were surface-functionalized by a modified copper-catalyzed azide-alkyne cycloaddition (CuAAC click reaction)[14, 32] of the surface-bound peptide 6-azido-lysine-cysteine-asparagine K($N_3$)CD with alkyne-functionalized molecular tweezers (Figure 2).

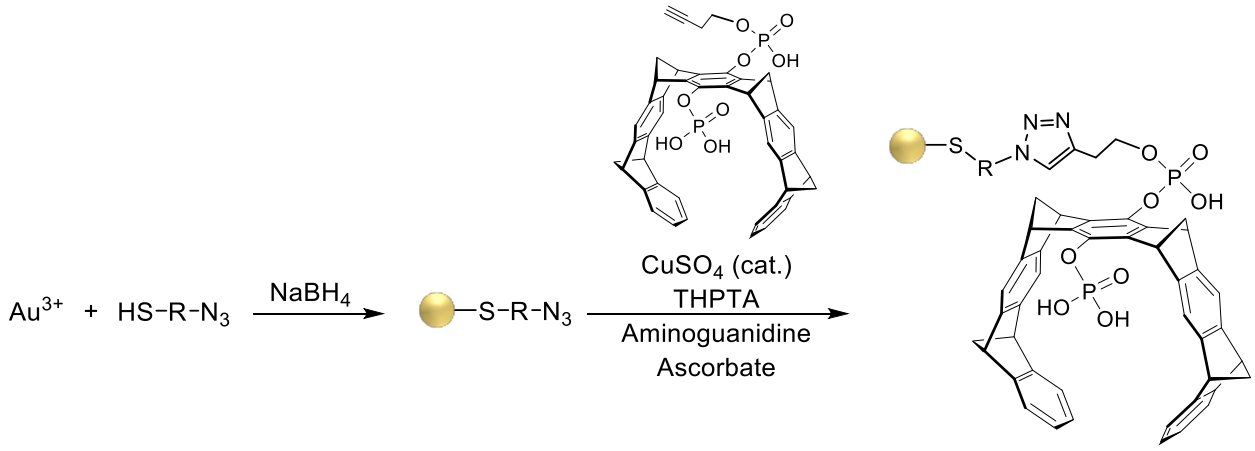


**Figure 2:** Synthetic pathway to tweezer-conjugated ultrasmall gold nanoparticles (Au-KCD-Tweezer) by clicking a butynyl-functionalized tweezer to an azide-terminated ultrasmall gold nanoparticle (Au-$N_3$). R = K($N_3$)CD.

Differential centrifugal sedimentation (DCS) gave a hydrodynamic diameter of $1.5 \pm 0.6$ nm for azide-terminated (Au-$N_3$) and of $1.4 \pm 0.5$ nm for tweezer-conjugated gold nanoparticles (Au-KCD-Tweezer; Figure 3). Note that the ligand shell on the particles generally has a considerable impact on the effective density, particularly for ultrasmall nanoparticles: A decrease in the effective density leads to a lower sedimentation rate and a systematic underestimation of the hydrodynamic particle diameter.[62] Consequently, the nanoparticles appear considerably smaller in DCS than they actually are. The difference between azide-terminated and tweezer-conjugated gold nanoparticles was not statistically significant. Dynamic light scattering (DLS) did not give reliable results due to the very small particle size.

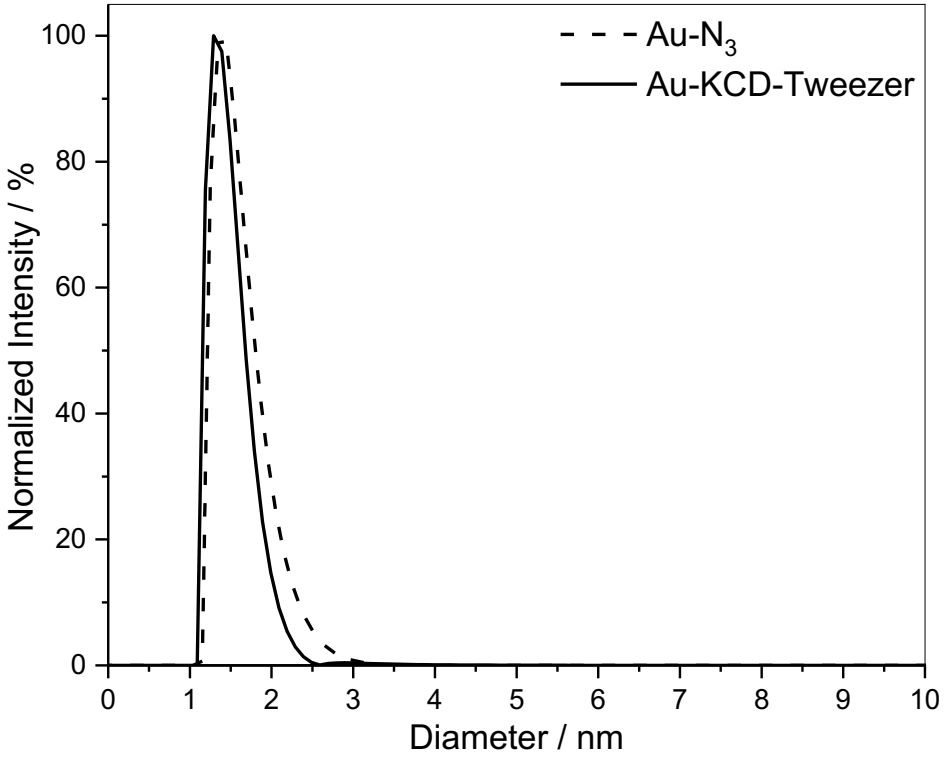


**Figure 3:** Differential centrifugal sedimentation curve of azide-terminated gold nanoparticles (Au-$N_3$) and of tweezer-conjugated gold nanoparticles (Au-KCD-Tweezer).

UV-VIS spectroscopy confirmed the binding of the tweezer molecules to the gold nanoparticles and allowed their quantification (absorption band at 280 nm; Figure 4). Note that these nanoparticles are too small to show surface plasmon resonance,[13, 63] therefore we do not see an absorption peak around 500 nm.

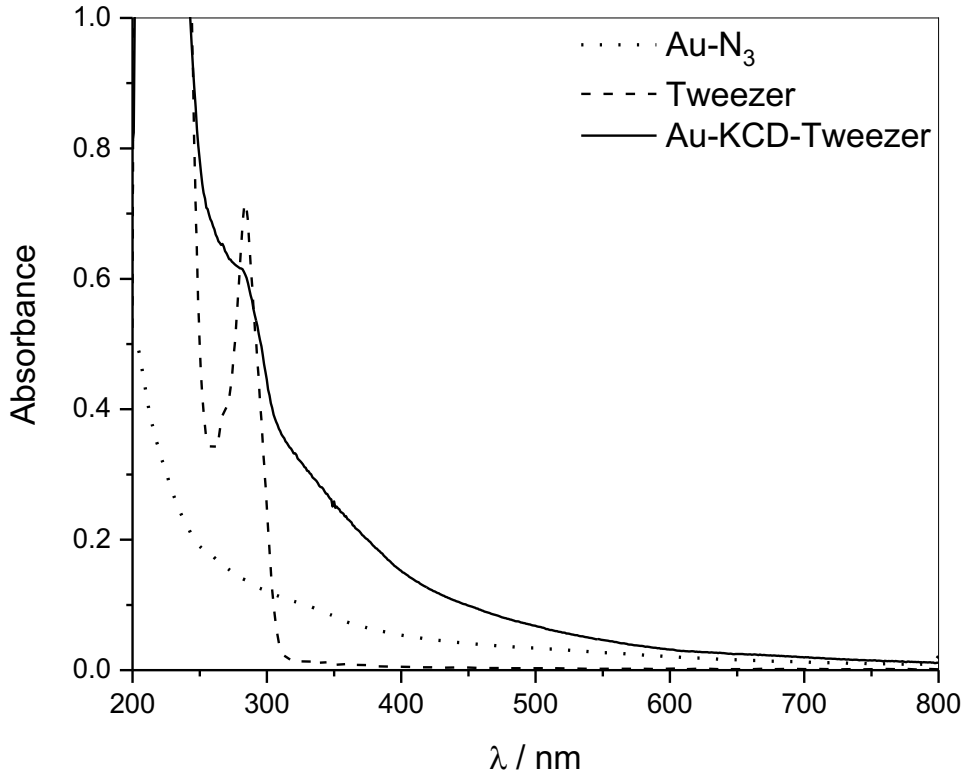


**Figure 4:** UV-VIS spectra of azide-terminated gold nanoparticles (Au-$N_3$, $c$(Au) = 22 µg $mL^{-1}$), of tweezer-conjugated gold nanoparticles (Au-KCD-Tweezer, $c$(Au) = 47 µg $mL^{-1}$), and of the dissolved tweezer alone ($c$(tweezer) = 67 µg $mL^{-1}$). The solvent was water in all cases. The absorption band (shoulder) at 280 nm shows the successful attachment of the tweezer to the gold nanoparticle and permits its quantification.

The size of the gold core and its shape were assessed by high-resolution transmission electron microscopy (HRTEM; Figure 5). TEM showed uniform particles with an average diameter of 2.2 ± 0.4 nm, i.e. larger than by DCS, as expected due to the limitations of the DCS method (see above). The inset image shows an *fcc* polyhedron in the [110] zone axis orientation enclosed by (100) and (111) facets. Fourier transformation analysis gave the *d*-spacings of *fcc* elemental gold. The attached ligands were not visible in HRTEM due to the low scattering contrast of the organic

ligands. For comparison, the HRTEM diameter of the azide-terminated gold nanoparticles was $2.0 \pm 0.4$ nm,[32] i.e. the click reaction did not significantly influence the metallic core.

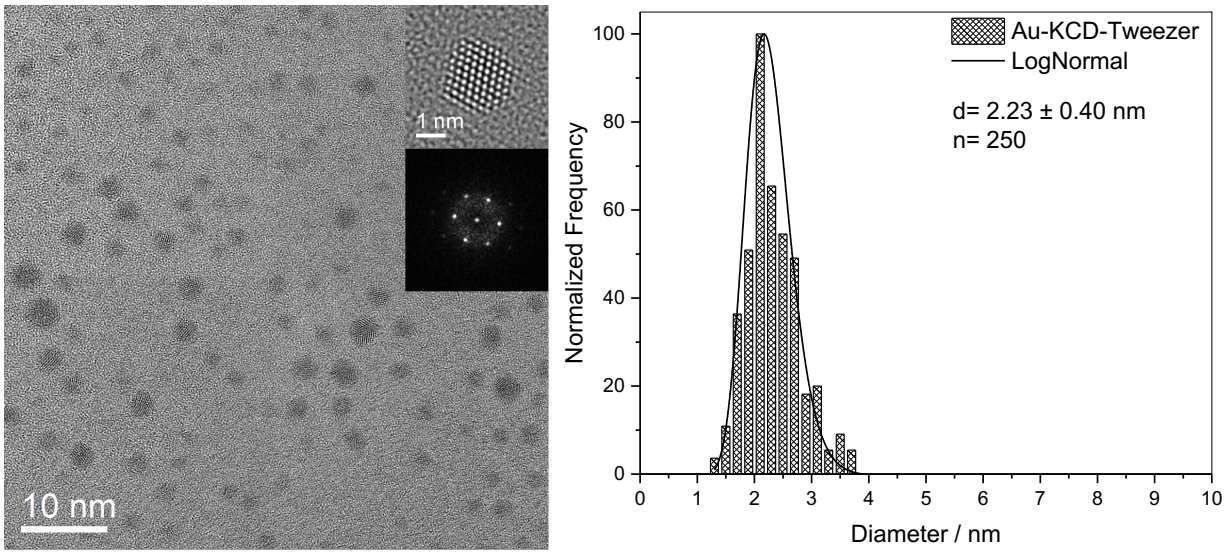


**Figure 5:** HRTEM image and Fourier transform insert of tweezer-conjugated ultrasmall gold nanoparticles (Au-KCD-Tweezer). The Fourier transformation clearly showed the [110] zone axis orientation of the single-crystalline *fcc* gold nanoparticle with $d(111) = 2.31$ Å in excellent agreement with the computed value of $d(111) = 2.35$ Å (**left**). The analysis of 250 particles gave a narrow particle size distribution (**right**).

The successful clicking of the monobutynyl tweezer to the gold nanoparticles was confirmed by $^1$H-NMR spectroscopy of dispersed nanoparticles (Figure 6). The major aromatic peaks of the nanoparticle-conjugated tweezer (6.5 to 7.8 ppm) were well pronounced after attachment, including the aromatic triazole proton from the click conjugation around 8 ppm. The observed strong line broadening compared to the free alkyne tweezer is consistent with the vicinity of the metallic nanoparticle

which broadens the NMR signals and has been observed previously for other ligands.[32, 33, 35, 36, 64] This analysis was only possible due to the ultrasmall nature of the nanoparticles; NMR spectroscopy of the ligand shell is not possible for larger nanoparticles at all. About 50% of the KCD-lysine residues carried an azide group (H9 at 3.35 ppm). The remaining fraction represents a regular KCD-lysine with a terminal $NH_3^+$ group, giving a signal for H9* at 3.0 ppm. The regular KCD peptide (i.e. lysine without azide group) was already present in the K(N3)CD peptide batch obtained from the supplier prior to its covalent attachment to the gold core, which was evident in the $^1$H and TOCSY NMR spectra of the peptide (not shown). The intensity ratio as determined by ERETIC[65] showed that about 50% of the KCD peptide carried an azide group after conjugation to the gold nanoparticle, giving about 117 ligands with an azide group and the same number with an amino group. Note that the peak at 3.0 ppm was attributed to the β-proton of the cysteine (H1) in an earlier publication.[32] A detailed investigation has now shown that this interpretation was not correct, and this wrong assignment is therefore corrected here. The signals of cysteine experience severe line broadening due to their vicinity to the gold core. Therefore, they are not visible close to the sharper signals of the remaining residues that are not directly bound to the gold core and also experience more internal molecular motion and therefore yield a narrower linewidth. Furthermore, overlap with signals from the other residues cannot be excluded.

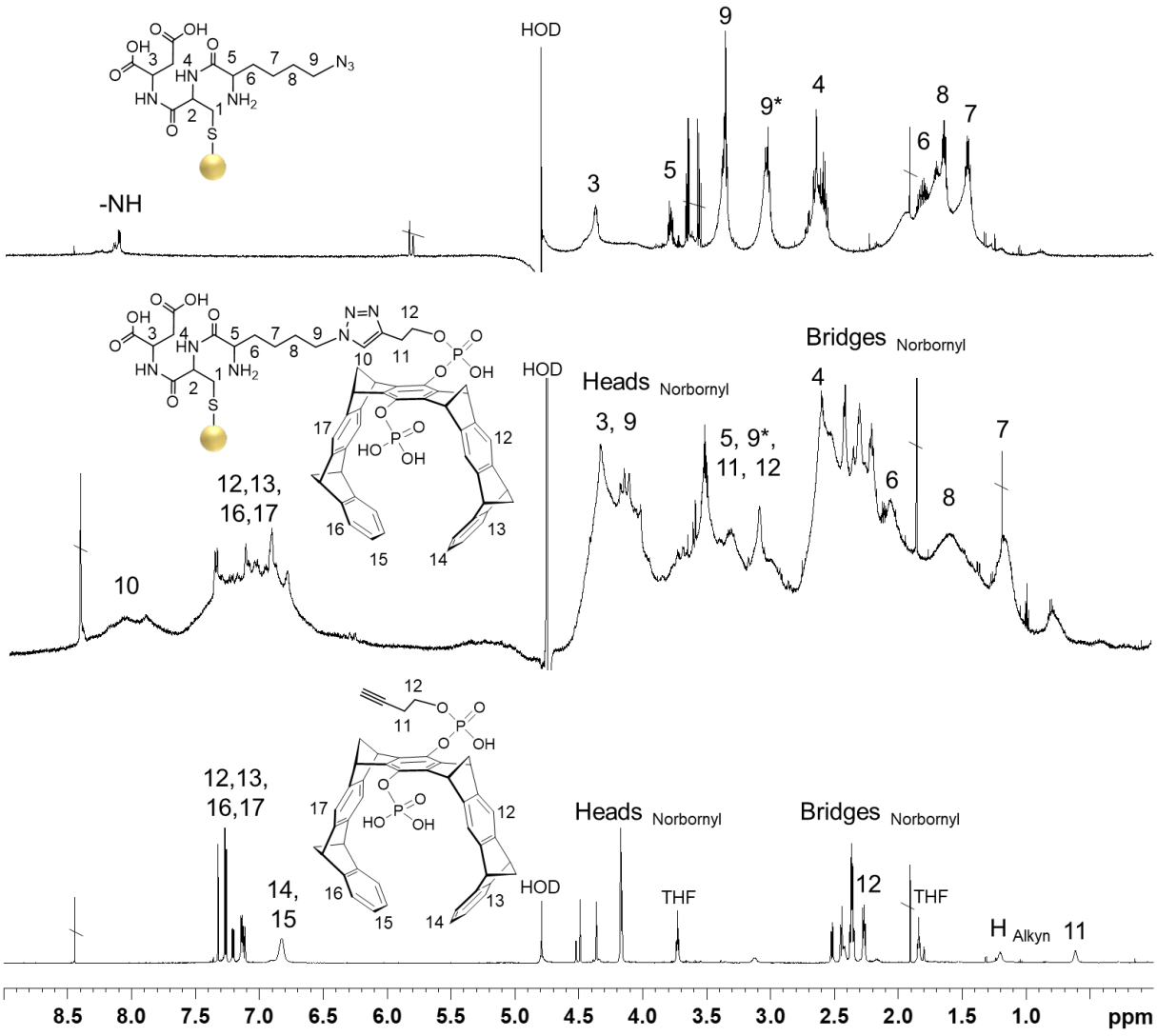


**Figure 6:** $^{1}$H-NMR spectra (700 MHz) of the azide-terminated gold nanoparticles (Au-$N_3$; **top**), of the tweezer-conjugated ultrasmall gold nanoparticles (Au-KCD-Tweezer; **center**), and of the dissolved monobutynyl tweezer (**bottom**), all measured in 10% $D_2O/H_2O$ at pH 8.

$^{1}$H-DOSY-NMR spectroscopy confirmed that the tweezer molecules were indeed attached to the gold nanoparticles as they diffused much more slowly than the free dissolved alkyne tweezer (Figure 7). The hydrodynamic diameter of the tweezer-conjugated nanoparticles was $2.9 \pm 1.3$ nm. For comparison, the hydrodynamic

diameter of the azide-terminated gold nanoparticles was 2.2 ± 02 nm,[32] and the hydrodynamic diameter of dissolved tweezer molecules was 1.4 ± 0.3 nm.

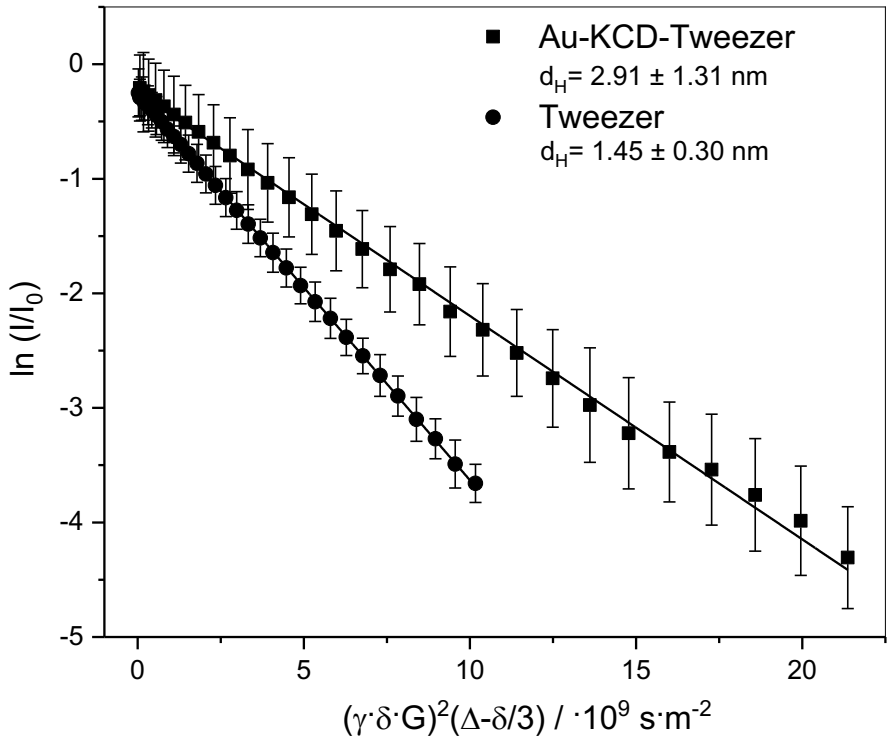


**Figure 7:** Stejskal-Tanner plots of dissolved tweezer molecules (dots) and tweezer-clicked gold nanoparticles (Au-KCD-Tweezer; squares). The diffusion coefficient of dissolved tweezer molecules and tweezer-clicked gold nanoparticles, respectively, equals the absolute value of the slope.

The concentration of nanoparticles was determined by measuring the gold concentration by AAS, followed by computing the mass of one gold nanoparticle, based on an average diameter of 2 nm, containing the corresponding number of gold atoms.[32] No copper from the click reaction was detected by AAS, i.e. the catalyst was completely removed by the washing steps after the click reaction. The tweezer concentration of the sample was measured by UV-VIS spectroscopy. Together with

the nanoparticle concentration calculated from the AAS data, we computed that between 11 and 30 tweezer molecules were attached to each gold nanoparticle (diameter 2 nm), depending on the synthesis batch. The reason for this variation is unknown and probably due to slight variations during the synthesis. Consequently, the surface density of tweezers on nanoparticles was determined separately for each synthetic batch.

A number of 11 to 30 tweezer molecules per nanoparticle (2 nm) gives a surface density between 0.9 and 2.4 tweezer molecules per $nm^2$ (footprint 0.42 to 1.14 $nm^2$ per tweezer). 117 azide molecules plus 117 lysine molecules were present on the surface of each nanoparticle (18.6 molecules per $nm^2$; footprint each 0.053 $nm^2$). This indicates that between 10 and 25% of the azide groups were accessed by the click reaction. This is in good agreement with earlier results on ligands on ultrasmall nanoparticles, i.e. clicked FAM (fluorescein; 8 to 9 molecules per 2 nm gold nanoparticle; 0.6 to 0.7 molecules per $nm^2$; footprint 1.48 $nm^2$),[14, 32] clicked Cy3 (5 molecules per 2 nm gold nanoparticle; 0.4 molecules per $nm^2$; footprint 2.5 $nm^2$)[14], and cysteine (67 molecules per 1.78 nm gold nanoparticle; 6.7 molecules per $nm^2$; footprint 0.15 $nm^2$).[36] Table 1 summarizes all characterization data. These gold particle concentrations (all based on an average diameter of 2 nm) and the derived tweezer concentrations were used for the interpretation of the NMR and ITC experiments described in the following.

**Table 1:** Particle size and ligand quantification data of all prepared nanoparticles. Note that DCS systematically underestimates the particle size. HRTEM gives the diameter of the metallic gold core, and $^{1}$H-NMR DOSY gives the hydrodynamic diameter of water-dispersed nanoparticles. All results confirm the stability of the gold core during the surface functionalization reactions.

| Particle | Diameter by DCS / nm | Diameter by HRTEM / nm | Diameter by $^{1}$H-NMR DOSY / nm | Composition |
|---|---|---|---|---|
| Dissolved K($N_3$)CD (free azide ligand)[32] | - | - | 1.5 ± 0.2 | - |
| Azide-terminated gold nanoparticles (Au-$N_3$)[32] | 1.5 ± 0.6 | 2.0 ± 0.4 | 2.2 ± 0.2 | 117 azide groups and 117 lysine groups per nanoparticle (2 nm; by $^{1}$H NMR spectroscopy) |
| Tweezer-conjugated gold nanoparticles (Au-KCD-Tweezer) | 1.4 ± 0.5 | 2.2 ± 0.4 | 2.9 ± 1.3 | 11 to 30 tweezer molecules per nanoparticle (2 nm; by UV-VIS spectroscopy) |
| Dissolved monobutynyl tweezer | - | - | 1.5 ± 0.3 | - |

It is possible that steric hindrance of multiple tweezers on the nanoparticle surface affects their recognition ability. Furthermore, the K($N_3$)CD peptide was only about 50% azide-functionalized, with the other half carrying unmodified lysine side chains, and thus these unmodified peptides were also present on the nanoparticle surface, in addition to the tweezer-clicked peptides. In principle, this could lead to an intramolecular binding of a tweezer to a lysine on the same nanoparticle or a

crosslinking between two nanoparticles (tweezer – lysine). To assess whether the surface-conjugated tweezers were still able to bind to lysine as model compound, we monitored the binding of the tweezer-conjugated nanoparticles to dissolved $^{13}C$,$^{15}N$-labeled lysine by NMR titration. In the following we demonstrate that the nanoparticle-conjugated tweezers do not bind to one of these unmodified lysine side chains on the same or on another nanoparticle.

For supramolecular tweezers binding to lysine and arginine, the largest change in the chemical environment occurs for the atoms at the end of the side chain that are inserted into the electron-rich aromatic tweezer cavity. We previously established a lysine-selective H2(C)N experiment which correlates the terminal lysine $CH_2$ group ($H_\varepsilon$) with the side chain nitrogen atom ($N_\zeta$) as a tool to distinguish and rank multiple tweezer binding sites within one protein in a semiquantitative way.[54, 58] Here we expand this technique to complex multiavid ligands like the tweezer-functionalized nanoparticles. Binding of tweezers to lysine and arginine occurs on the intermediate-to-fast time scale which results in strong line broadening and thus a loss of signal intensity, even at very low tweezer concentrations and before a significant signal shift takes place.[54] Consequently, the lysine NMR signal has already broadened to disappearance well below a molar 1:1 ratio of tweezer to lysine (Figure 8). A similar signal broadening was observed when titrating dissolved diphosphate tweezers to lysine.[54] If the unreacted lysines present on the nanoparticle surface (which are invisible in this NMR experiment) would significantly compete with the visible, isotope labeled-lysine, the line broadening would be expected to be much less pronounced and to occur at much higher ligand concentrations. As this is not the case, we conclude that the clicked tweezers on the gold nanoparticle surface were able to act as lysine binders, and that the remaining lysine residues on the nanoparticle surface from the K($N_3$)CD ligand did not interfere with this binding

process. In addition, the free monobutynyl tweezer was added to the Au-$N_3$ nanoparticles in a control $^1$H-NMR titration to test whether the tweezer can bind the lysine side chains on the nanoparticle. Line broadening of the nanoparticle signals only occurred at tweezer concentrations much higher compared to titrating tweezer to free lysine,[41] without shifting of the signals. This is probably due to non-specific electrostatic interactions and a 'walking' of the tweezer on the nanoparticle surface like it was observed for proteins with many lysines on the surface.[66] Since on nanoparticles with covalently attached tweezers the tweezers cannot walk and still bind to external lysines, these effects on the Au-$N_3$ nanoparticles are not a concern for the subsequent protein binding studies.

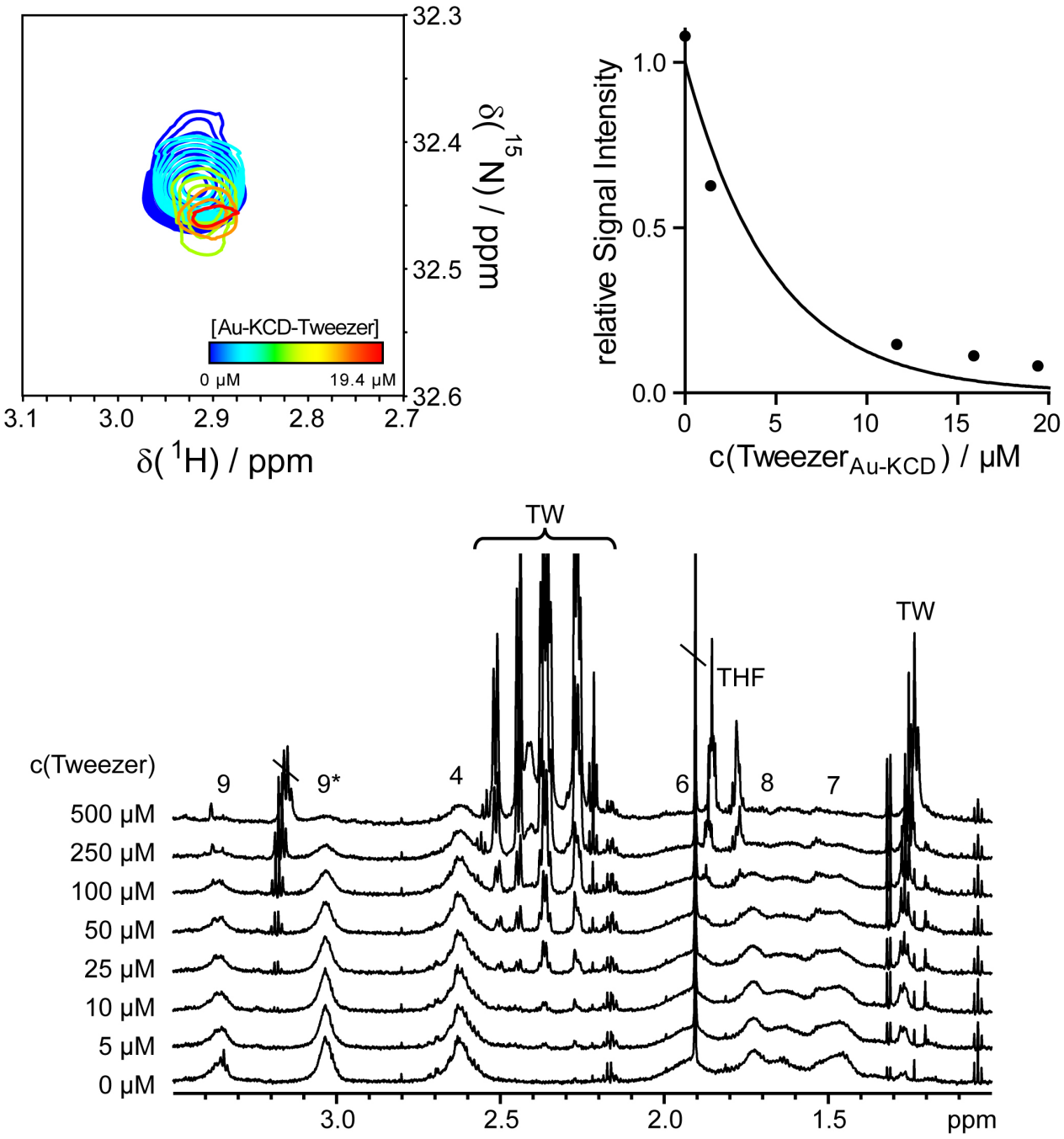


**Figure 8: Top:** H2(C)N NMR spectra of the titration of dissolved $^{15}N^{13}C$-labeled lysine (300 µM, 50 mM KPi buffer at pH 8) with tweezer-conjugated gold nanoparticles (Au-KCD-Tweezer), recorded at 700 MHz. Spectral overlay (**left**) and plot of relative signal intensities against the tweezer concentration (on Au-KCD-Tweezer nanoparticles) (**right**) are shown. The peak broadening and the resulting

decay in the signal intensity are indicative of the tweezer binding to lysine. The final concentration of nanoparticle-bound tweezers (19.4 μM) corresponds to a 1:10 molar ratio of tweezers to lysine. **Bottom:** $^{1}$H-NMR titration of Au-$N_3$ nanoparticles with monobutynyl tweezer. Some line broadening is observed at much higher concentrations compared to tweezer binding to free lysine. All signals broaden and no signal shifts are observed, indicating a non-specific electrostatic interaction of the tweezer with the nanoparticle at high concentrations, but little to no encapsulation of a lysine side chain in the tweezer cavity.

After having confirmed the targeting ability of the tweezers bound to the nanoparticles, the binding to lysine and arginine on the surface of proteins was investigated. We chose the WW domain of the human peptidyl prolyl *cis-trans* isomerase (PPIase) hPin1 as first model system. The hPin1-WW domain (4.5 kDa; hPin1-WW) consists of 36 amino acids, including two lysines and four arginines. Its interaction with free diphosphate tweezers has been thoroughly investigated by NMR.[54] In addition to the two lysines, the N-terminal glycine Hα/N correlation is also visible in the lysine H2(C)N spectrum.[54] Tweezer-functionalized gold nanoparticles were titrated with $^{13}$C,$^{15}$N-labelled hPin1-WW, recording both lysine- and arginine-specific H2(C)N spectra of the protein (Figure 9).

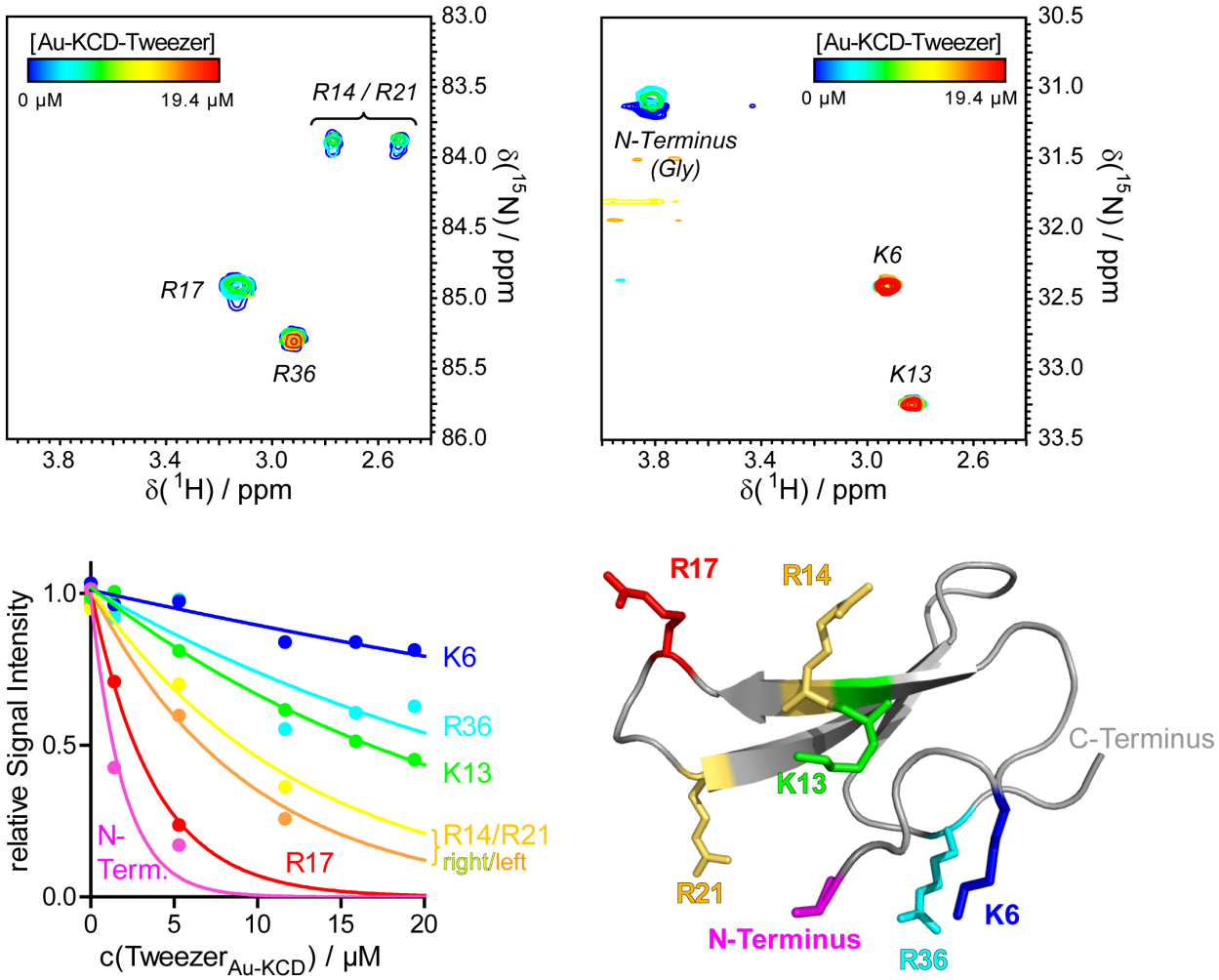


**Figure 9:** H2(C)N spectra of the arginine residues R14, R17, R24, R36 (**top left**; signals of R14 and R21 are both split and overlapped) and the lysine residues K6, K13 (**top right**) of the $^{13}C$,$^{15}N$-labelled hPin1-WW domain (300 µM) at increasing concentrations of tweezer-conjugated ultrasmall gold nanoparticles (Au-KCD-Tweezer). The final concentration of nanoparticle-bound tweezers (19.4 µM) corresponds to a 1:10 molar ratio of tweezer to protein. A decrease in signal intensity indicated binding, with preferred binding sites showing a faster decay. The plot of signal intensities versus the nanoparticle-bound tweezer concentration (**bottom left**) showed the fastest intensity decay for the N-terminus and for R17, indicating a preferred binding at these sites. **Bottom right**: Binding sites mapped onto the hPin1-

WW domain structure (PDB No. 2M8I) with the same color code as in the intensity plot; lysine and arginine residues are shown as sticks.

Because these experiments are so sensitive even at sub-stoichiometric ligand concentrations, they are well suited to monitor the binding event of the Au-KCD-Tweezer nanoparticles, although a stoichiometric ratio could not be achieved due to the high protein concentrations needed. In earlier experiments with dissolved phosphate tweezers and hPin1, a distinct binding order was obtained from the rates of signal decay in the H2(C)N spectra: The signal of R17 broadened and disappeared at very low tweezer concentrations, while the R36 and the N-terminal glycine signals remained nearly unchanged, giving a binding order of R17 >> K6 ≈ R14 ≈ R21 > K13 >> R36.[54]

Interestingly, a considerably different binding order was observed with the tweezer-conjugated nanoparticles: N-terminus (G) ≈ R17 > R21/R14 > K13 > R36 > K6. The R17 signal in the H2(C)N spectrum broadened first as with free tweezers, but the N-terminus (which was not bound by the free tweezers at all) showed a strong line broadening at low ligand concentrations as well. The mechanism by which the N-terminal glycine residue is bound remains open. It is unlikely that it can be inserted into the tweezer cavity because it is too short, but the observed changes may result from a hydrogen bond to the KCD peptide scaffold in the vicinity of the covalently attached tweezers. It is unlikely that this behavior is caused by allosteric changes since the N-terminus is flexible and unstructured (pdb 2M8I). Furthermore, K6 was affected least by the nanoparticles, although it was well bound by free tweezer molecules.[54]

Only sub-stoichiometric tweezer concentrations could be investigated because the H2(C)N experiments required a high protein concentration and the available amounts

of nanoparticles were limited. Therefore, we performed an $^{15}$N-HSQC titration of $^{15}$N-labeled hPin1-WW which required a lower protein concentration so that an excess of tweezers to protein was achieved. The $^{15}$N-HSQC spectra show the correlation of the amide H and N, as well as some side chain NH correlations. Ligand binding results in a signal shift and also some line broadening for residues close to the binding site.

Titrating the free monobutynyl tweezer to $^{15}$N-hPin1-WW (Figure 10) resulted in a shift of signals in the region between residues 15-22, including the two arginine residues R17 and R21. For the Au-KCD-Tweezer nanoparticles, shifts were observed for the same signals, which confirmed the preference for R17 observed in the H2(C)N experiments (Figure 11). The most striking difference compared to the free monobutynyl tweezer was a strong intensity loss due to line broadening of multiple signals, which led to their complete disappearance. Therefore, chemical shift perturbations could only be qualitatively assessed. The signal decay curves for the lysine and arginine residues (Figure 11, bottom left) and the ligand concentration at which each signal disappeared completely (Figure 11, bottom right) showed that the region between R17 and R21 responded to very low nanoparticle concentrations, confirming it as the preferred binding site. The observed line broadening could point to a shift of the binding equilibrium from fast to intermediate exchange, which implies a tighter binding of the nanoparticle compared to free tweezers. An exchange between different tweezer molecules of the same nanoparticle ('walking' or 'rolling') could also account for the low signal intensities at the preferred binding sites.

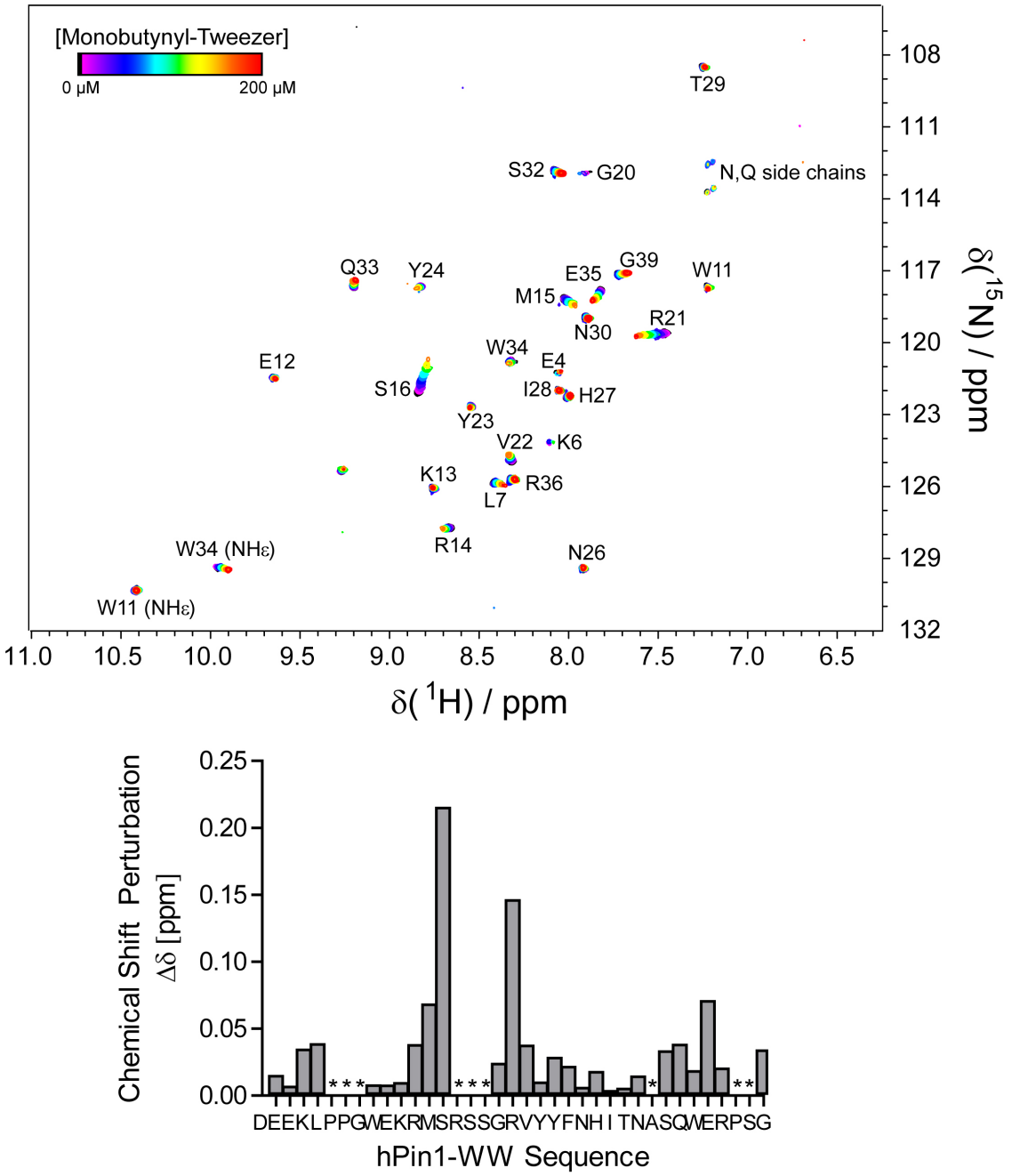


**Figure 10:** $^{15}$N-HSQC titration of $^{15}$N-hPin1-WW (50 µM, 50 mM KPi buffer at pH 8) with dissolved monobutynyl tweezer. Spectra overlay (**top**) and chemical shift perturbations (**bottom**) plotted against the protein sequence for 150 µM tweezer. Amino acids that are not visible in the HSQC spectrum are labeled with *.

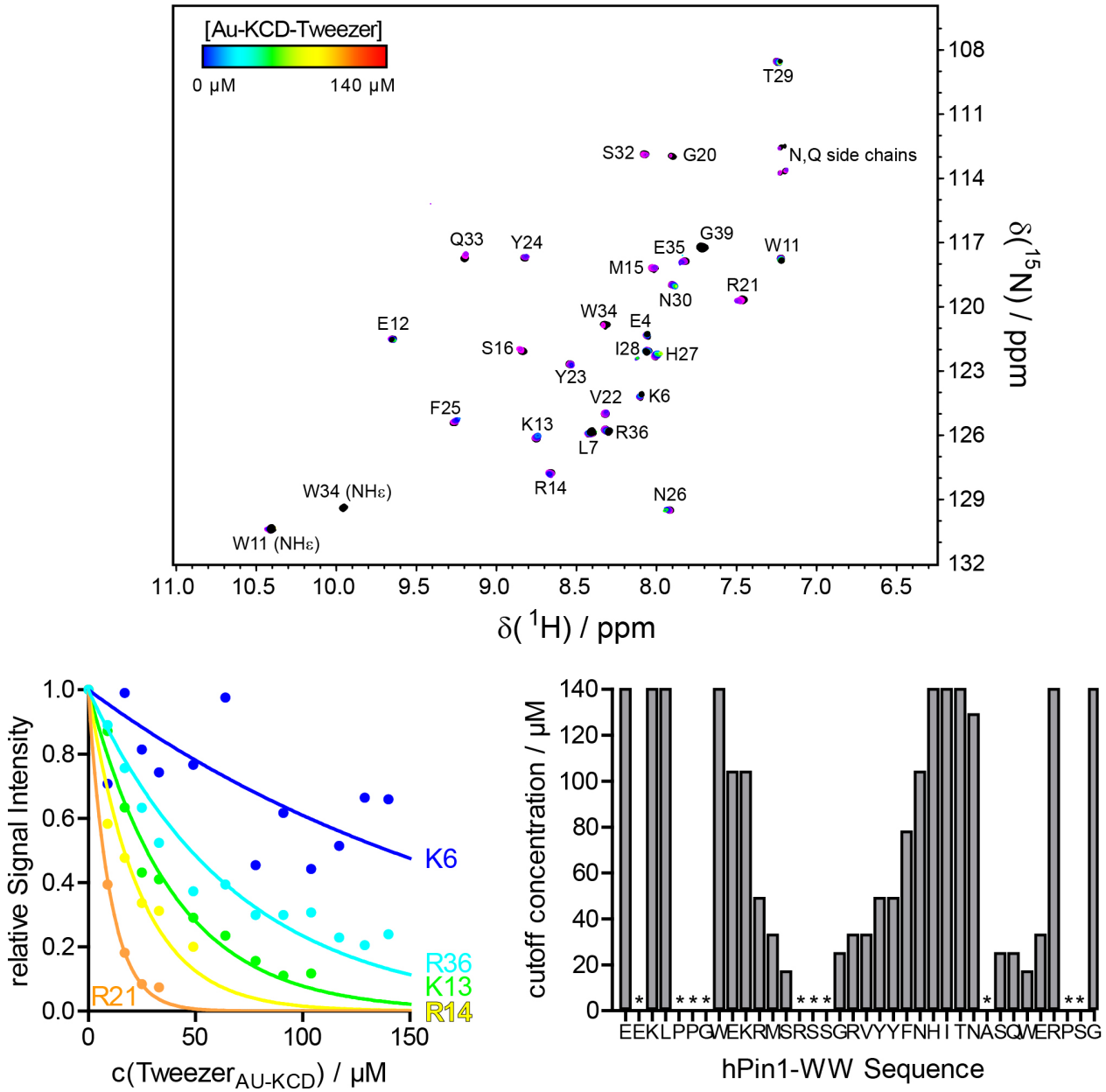


**Figure 11:** $^{15}$N-HSQC NMR titration of the hPin1-WW domain (50 µM, 50 mM KPi buffer at pH 8) with tweezer-conjugated ultrasmall gold nanoparticles (Au-KCD-Tweezer) recorded at 700 MHz (**top**). The signals of the two tryptophane indole NHs are labelled with NHε. Signal shifts and reduced intensities indicate binding. The plot of signal intensities against nanoparticle-bound tweezer concentration (**bottom left**, shown for lysine and arginine residues only) showed the same order of binding

as in the H2(C)N experiments (Figure 9). R17 and the N-terminus were not visible in the HSQC spectrum. A plot of the cutoff concentrations (**bottom right**, last concentration where a signal is still visible) against the hPin1-WW sequence indicated preferred binding to R17 and R21 as shown by the low cutoff concentrations. Amino acids that are not visible in the HSQC spectrum are labeled with an asterisk *.

In summary, the H2(C)N and HSQC NMR experiments point to R17 as preferred binding site for both nanoparticle-conjugated tweezers and free tweezers. Interestingly, the order of binding observed in the H2(C)N spectra is different between nanoparticles and free tweezers, which likely reflects an increased multiavid binding in favor of lysine and arginine residues in the vicinity of R17. K6, which ranks lower in the preferred binding hierarchy of the nanoparticles, lies on the opposite side of the protein. While free tweezers can bind K6 in addition to other sites without steric hindrance, tweezers on the same particle that binds to R17 cannot reach K6, and the size of the tweezer-decorated nanoparticle might be too large to accommodate a second one binding on the K6 side of hPin1-WW. The line broadening in the HSQC titration of the nanoparticles can also be attributed to their multiavid nature, but more structural details of this interaction cannot be derived from the collected data. We tentatively attribute the observed differences to the fact that the tweezers clicked to a nanoparticle surface show a distinct binding pattern with a potential multiavidity (more than one tweezer on a given nanoparticle binds to the same protein molecule) but also to steric hindrance due to the larger size of the nanoparticle compared to free tweezers.

For a more quantitative assessment of binding, an ITC titration of hPin1-WW to tweezer-conjugated nanoparticles was performed. However, data analysis of such a

complex system involving a multiavid ligand binding to a protein with multiple potential binding sites with possibly different binding constants, is challenging. Due to the lack of a good model describing the binding equilibria and the risk of overfitting, the titrations were fitted with the simplest model that provided a good fit of the data (stochiometric equilibria approach/simple model by AFFINImeter). This model assumes that protein and tweezer form a 1:1 complex. We opted to use the concentration of the tweezer units rather than gold cores because this yielded reasonably well fitted binding curves. This in turn implies 11 to 30 tweezers on each nanoparticle independently binding to a protein, which appears unlikely to due steric hindrance. Therefore, the observed $K_D$ values reflect the correct order of magnitude, but the absolute value has to be taken with care and experimental stoichiometries could not be determined.

Binding of hPin1-WW to tweezer-conjugated nanoparticles resulted in an exothermic binding reaction with a dissociation constant of $K_D = 41 \pm 2$ μM (Figure 12). A control titration of the hPin1-WW domain with azide-terminated gold nanoparticles caused only small endothermic peaks (Figure 13). Hence, an unspecific binding of the protein to the nanoparticles can be excluded. For comparison, a $K_D$ of $12 \pm 2$ μM was determined for the interaction of free phosphate tweezers with hPin1-WW with a multiple-site binding model by ITC.[54]

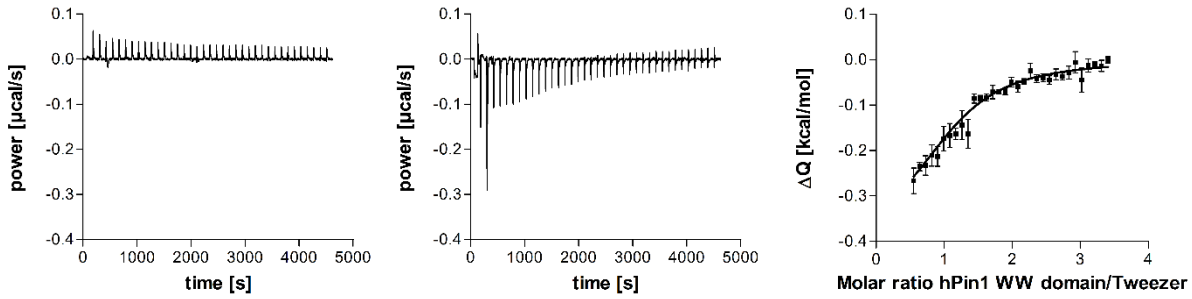


**Figure 12:** hPin1-WW binds to tweezer-conjugated gold nanoparticles (Au-KCD-Tweezer) as shown by ITC. 3.5 mM hPin1-WW domain was titrated to tweezer-conjugated or azide-terminated nanoparticles (Au-$N_3$) in 50 mM KPi, 90 mM KCl, pH 8.0 at 25 °C. **Left**: Processed heating power over time from hPin1-WW titration to azide-terminated gold nanoparticles (Au-$N_3$; control). **Centre**: Processed heating power over time from hPin1-WW domain titration to tweezer-conjugated gold nanoparticles (Au-KCD-Tweezer). **Right**: Integrated energy values over molar ratio of protein and tweezer. All data were processed and fitted with the simple model stoichiometric approach with the software AFFINImeter. The first three data points were excluded from the analysis.

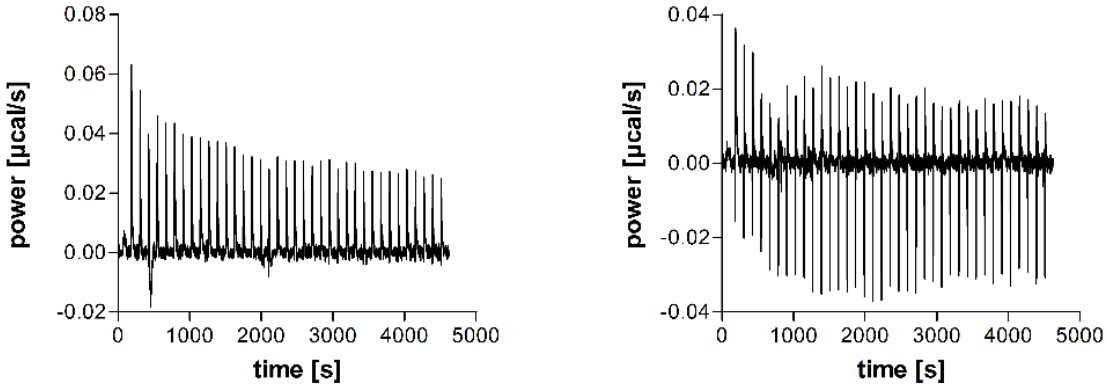


**Figure 13:** Magnification of the control experiments by ITC from Figure 12, showing the unspecific interaction between azide-terminated gold nanoparticles (au-$N_3$) with hPin1 WW (**left**) und Survivin (**right**).

Finally, binding of the tweezer-conjugated nanoparticles to the larger protein Survivin, an interesting cancer target, was measured by ITC (Figure 14). The tweezer-conjugated gold nanoparticles gave much larger exothermic peaks compared to azide-terminated gold nanoparticles, which indicates a stronger interaction with Survivin and underscores that an unspecific nanoparticle-protein binding is not present (Figure 13). The ITC titration of Survivin to the tweezer-conjugated nanoparticles resulted in a dissociation constant $K_D = 8 \pm 1$ µM with a fixed 1:1 stoichiometry of protein to tweezer. For comparison, the dissociation constant of unconjugated phosphate tweezers to Survivin was $38 \pm 4$ µM (unpublished). These values contrast with higher affinities determined earlier for single tweezer molecules on the surface of p97's N domain (6 µM).[39] and 14-3-3 proteins (30 µM).[42] However, especially the biphasic curves obtained from 14-3-3 titration with tweezers document that that their affinity to any given lysine or arginine on a protein surface is strongly affected by topographical factors like steric accessibility, local surface potential, positively charged neighbor residues, and

hydrophobic or aromatic interactions.[39, 42, 54] Thus, tweezer affinities not only vary between different proteins, but also between basic residues of the same protein.

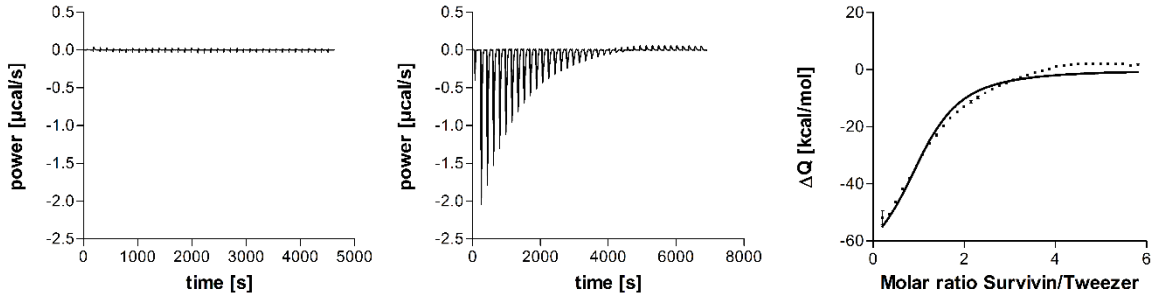


**Figure 14:** Survivin binds to tweezer-conjugated gold nanoparticles as shown by ITC. 1.2 mM Survivin was titrated to tweezer-conjugated or azide-terminated nanoparticles in PBS, pH 7.4, at 25 °C. **Left**: Processed heating power over time from ITC titration of Survivin to azide-terminated gold nanoparticles (Au-$N_3$; control). **Centre**: Processed heating power over time from Survivin titration to tweezer-conjugated gold nanoparticles (Au-KCD-Tweezer). **Right**: Integrated energy values over molar ratio of protein and tweezer. The data were processed and fitted using the simple model stoichiometric approach of the software AFFINImeter. The deviation between data and fit indicates that multiple binding events are present, but since there is no clear plateau between the phases ($K_{DS}$ are too similar), it was not possible to obtain reliable parameters from a multi-step binding model.

## Conclusions

In this work, we demonstrated how multiple selective supramolecular ligands can be covalently attached to ultrasmall nanoparticles and investigated their unique binding behaviour towards two model proteins. Employing click chemistry, alkyne-

functionalized molecular tweezer molecules can be covalently attached to the surface of azide-containing ultrasmall gold nanoparticles (2 nm). Each nanoparticle carries about 11-30 tweezer molecules. NMR spectroscopic investigations with the model protein hPin1-WW show that molecular tweezers, clicked onto the surface of the nanoparticles, are able to specifically interact with amino acids on the protein surface. A competition to protein binding by remaining free lysine side chains on the nanoparticle surface could be excluded. Clearly, the binding properties of the tweezers to attach to lysine and arginine, both free and on a protein surface, are still present after attaching them to a nanoparticle.

The specific interaction of the new nanoparticle tweezer conjugates with proteins was quantitatively assessed by NMR spectroscopy and isothermal titration calorimetry (ITC) with hPin1 and Survivin. In contrast to dissolved tweezer molecules, the particle-bound tweezers not only bind to the lysine and arginine residues within the hPin1-WW domain, but also interact strongly with the glycine residue of the N-terminus or its immediate vicinity. For both model systems, the tweezer-conjugated nanoparticles bind to the protein with a comparable affinity with respect to the free tweezers. Generally, for a multiavid ligand a tighter binding compared to its monoavid version is expected. However, this assumes that all ligands can reach their protein receptor site at the same time. For the nanoparticles, this is probably not the case because the tweezer ligands are distributed in a spherical geometry and therefore not all of them will be able to reach the protein surface at the same time.

A possible gain in binding affinity will therefore greatly depend on the topology and positioning of lysine and arginine residues on a specific target protein surface. While an advantage of the nanoparticle conjugate over free tweezers might not be obvious from the $K_D$ values alone, there are two interesting features of the nanoparticles

which we will explore in the future: The size of a tweezer-conjugated nanoparticle is much larger compared to a single tweezer molecule. Therefore, it is possible to cover and thus block a larger epitope on the protein surface which can be favorable when aiming to inhibit protein-protein interactions. Furthermore, the multiavidity of the nanoparticle system offers the possibility to attach more than one ligand type on a single particle. The ligand density on the nanoparticle could also be varied by mixing tweezers with "space holder" ligands like cysteine. This also opens up the possibility to improve affinity and selectivity by combining different recognition units (heteroavidity).

Finally, covalently functionalized ultrasmall gold nanoparticles, decorated with supramolecular binders, may be well suited to target proteins both inside and outside cells, because they have the potential to enter cells and in favorable cases also the cell nucleus.

**Acknowledgements**

The authors acknowledge financial support by the Deutsche Forschungsgemeinschaft (DFG) in the framework of the Collaborative Research Centre CRC 1093: Supramolecular Chemistry on Proteins. We thank Dr. Torsten Schaller and Dr. Felix Niemeyer for experimental assistance with NMR spectroscopy and Peter Binz for technical support. We thank Kerstin Brauner and Robin Meya for elemental analyses. We thank Anna-Lena Bünte for experimental assistance and Alma Rute for preparation of hPin1-WW. We thank Prof. Hemmo Meyer for access to the ITC equipment.

## References


1. Vallet, C.; Aschmann, D.; Beuck, C.; Killa, M.; Meiners, A.; Mertel, M.; Ehlers, M.; Bayer, P.; Schmuck, C.; Giese, M., et al., Functional disruption of the cancer-relevant interaction between survivin and histone H3 with a guanidiniocarbonyl pyrrole ligand. *Angew. Chem. Int. Ed. Engl.* **2020,** *59*, 5567-5571.
2. Hadrovic, I.; Rebmann, P.; Klärner, F. G.; Bitan, G.; Schrader, T., Molecular lysine tweezers counteract aberrant protein aggregation. *Front. Chem.* **2019,** *7*, 657-657.
3. Kubota, R.; Hamachi, I., Protein recognition using synthetic small-molecular binders toward optical protein sensing in vitro and in live cells. *Chem. Soc. Rev.* **2015,** *44*, 4454-4471.
4. Milroy, L. G.; Grossmann, T. N.; Hennig, S.; Brunsveld, L.; Ottmann, C., Modulators of protein–protein interactions. *Chem. Rev.* **2014,** *114*, 4695-4748.
5. Peczuh, M. W.; Hamilton, A. D., Peptide and protein recognition by designed molecules. *Chem. Rev.* **2000,** *100*, 2479-2494.
6. Kopp, M.; Kollenda, S.; Epple, M., Nanoparticle–protein interactions: Therapeutic approaches and supramolecular chemistry. *Acc. Chem. Res.* **2017,** *50*, 1383-1390.
7. Algar, W. R.; Jeen, T.; Massey, M.; Peveler, W. J.; Asselin, J., Small surface, big effects, and big challenges: toward understanding enzymatic activity at the inorganic nanoparticle–substrate interface. *Langmuir* **2019,** *35*, 7067-7091.
8. Ferreira, R. S.; Lira, A. L.; Torquato, R. J. S.; Schuck, P.; Sousa, A. A., Mechanistic insights into ultrasmall gold nanoparticle-protein interactions through measurement of binding kinetics. *J. Phys. Chem. C* **2019,** *123*, 28450-28459.
9. Scaletti, F.; Hardie, J.; Lee, Y. W.; Luther, D. C.; Ray, M.; Rotello, V. M., Protein delivery into cells using inorganic nanoparticle-protein supramolecular assemblies. *Chem. Soc. Rev.* **2018,** *47*, 3421-3432.
10. Boselli, L.; Polo, E.; Castagnola, V.; Dawson, K. A., Regimes of biomolecular ultrasmall nanoparticle interactions. *Angew. Chem. Int. Ed.* **2017,** *56*, 4215-4218.
11. Rotello, V. M., Organic chemistry meets polymers, nanoscience, therapeutics and diagnostics. *Beilstein J. Org. Chem.* **2016,** *12*, 1638-1646.
12. Jiang, Y.; Wang, M.; Hardie, J.; Tonga, G. Y.; Ray, M.; Xu, Q.; Rotello, V. M., Chemically engineered nanoparticle-protein interface for real-time cellular oxidative stress monitoring. *Small* **2016,** *12*, 3775-3779.
13. Zarschler, K.; Rocks, L.; Licciardello, N.; Boselli, L.; Polo, E.; Garcia, K. P.; De Cola, L.; Stephan, H.; Dawson, K. A., Ultrasmall inorganic nanoparticles: State-of-the-art and perspectives for biomedical applications. *Nanomedicine* **2016,** *12*, 1663-1701.
14. Sokolova, V.; Nzou, G.; van der Meer, S. B.; Ruks, T.; Heggen, M.; Loza, K.; Hagemann, N.; Murke, F.; Giebel, B.; Hermann, D. M., et al., Ultrasmall gold nanoparticles (2 nm) can penetrate and enter cell nuclei in an in-vitro brain spheroid model. *Acta Biomater.* **2020,** *111*, 349-362.
15. Dzwonek, M.; Zalubiniak, D.; Piatek, P.; Cichowicz, G.; Meczynska-Wielgosz, S.; Stepkowski, T.; Kruszewski, M.; Wieckowska, A.; Bilewicz, R., Towards potent but less toxic nanopharmaceuticals - lipoic acid bioconjugates of ultrasmall gold nanoparticles with an anticancer drug and addressing unit. *RSC Adv.* **2018,** *8*, 14947-14957.
16. Yang, L.; Shang, L.; Nienhaus, G. U., Mechanistic aspects of fluorescent gold nanocluster internalization by live HeLa cells. *Nanoscale* **2013,** *5*, 1537-1543.

17. Leifert, A.; Pan-Bartnek, Y.; Simon, U.; Jahnen-Dechent, W., Molecularly stabilised ultrasmall gold nanoparticles: synthesis, characterization and bioactivity. *Nanoscale* **2013,** *5*, 6224-6242.
18. Huo, S.; Jin, S.; Ma, X.; Xue, X.; Yang, K.; Kumar, A.; Wang, P. C.; Zhang, J.; Hu, Z.; Liang, X. J., Ultrasmall gold nanoparticles as carriers for nucleus-based gene therapy due to size-dependent nuclear entry. *ACS Nano* **2014,** *8*, 5852-5862.
19. Zhang, X.; Shastry, S.; Bradforth, S. E.; Nadeau, J. L., Nuclear uptake of ultrasmall gold-doxorubicin conjugates imaged by fluorescence lifetime imaging microscopy (FLIM) and electron microscopy. *Nanoscale* **2015,** *7*, 240-251.
20. Elliott, E. W.; Ginzburg, A. L.; Kennedy, Z. C.; Feng, Z.; Hutchison, J. E., Single-step synthesis of small, azide-functionalized gold nanoparticles: versatile, water-dispersible reagents for click chemistry. *Langmuir* **2017,** *33*, 5796-5802.
21. Chen, Y. P.; Xianyu, Y. L.; Jiang, X. Y., Surface modification of gold nanoparticles with small molecules for biochemical analysis. *Acc. Chem. Res.* **2017,** *50*, 310-319.
22. Li, N.; Zhao, P.; Salmon, L.; Ruiz, J.; Zabawa, M.; Hosmane, N. S.; Astruc, D., "Click" star-shaped and dendritic PEGylated gold nanoparticle-carborane assemblies. *Inorg. Chem.* **2013,** *52*, 11146-11155.
23. Rousseau, G.; Fensterbank, H.; Baczko, K.; Cano, M.; Allard, E.; Larpent, C., Azido-coated nanoparticles: a versatile clickable platform for the preparation of fluorescent polystyrene core–PAMAM shell nanoparticles. *Macromolecules* **2012,** *45*, 3513-3522.
24. Baranov, D.; Kadnikova, E. N., Synthesis and characterization of azidoalkyl-functionalized gold nanoparticles as scaffolds for "click"-chemistry derivatization. *J. Mater. Chem.* **2011,** *21*, 6152-6157.
25. Thode, C. J.; Williams, M. E., Kinetics of 1,3-dipolar cycloaddition on the surfaces of Au nanoparticles. *J. Coll. Interf. Sci.* **2008,** *320*, 346-352.
26. Limapichat, W.; Basu, A., Reagentless functionalization of gold nanoparticles via a 3 + 2 Huisgen cycloaddition. *J. Coll. Interf. Sci.* **2008,** *318*, 140-144.
27. Gole, A.; Murphy, C. J., Azide-derivatized gold nanorods: Functional materials for "Click" chemistry. *Langmuir* **2008,** *24*, 266-272.
28. Fischler, M.; Sologubenko, A.; Mayer, J.; Clever, G.; Burley, G.; Gierlich, J.; Carell, T.; Simon, U., Chain-like assembly of gold nanoparticles on artificial DNA templates via 'click chemistry'. *Chem. Comm.* **2008**, 169-171.
29. Boisselier, E.; Salmon, L.; Ruiz, J.; Astruc, D., How to very efficiently functionalize gold nanoparticles by "click" chemistry. *Chem. Comm.* **2008,** (44), 5788-5790.
30. Fleming, D. A.; Thode, C. J.; Williams, M. E., Triazole cycloaddition as a general route for functionalization of Au nanoparticles. *Chem. Mater.* **2006,** *18*, 2327-2334.
31. Brennan, J. L.; Hatzakis, N. S.; Tshikhudo, T. R.; Razumas, V.; Patkar, S.; Vind, J.; Svendsen, A.; Nolte, R. J. M.; Rowan, A. E.; Brust, M., Bionanoconjugation via click chemistry: The creation of functional hybrids of lipases and gold nanoparticles. *Bioconjugate Chem.* **2006,** *17*, 1373-1375.
32. van der Meer, S. B.; Loza, K.; Wey, K.; Heggen, M.; Beuck, C.; Bayer, P.; Epple, M., Click chemistry on the surface of ultrasmall gold nanoparticles (2 nm) for covalent ligand attachment followed by NMR spectroscopy. *Langmuir* **2019,** *35*, 7191-7204.
33. Salassa, G.; Burgi, T., NMR spectroscopy: a potent tool for studying monolayer-protected metal nanoclusters. *Nanoscale Horiz.* **2018,** *3*, 8.

34. Konopka, C. J.; Wozniak, M.; Hedhli, J.; Ploska, A.; Schwartz-Duval, A.; Siekierzycka, A.; Pan, D.; Munirathinam, G.; Dobrucki, I. T.; Kalinowski, L., et al., Multimodal imaging of the receptor for advanced glycation end-products with molecularly targeted nanoparticles. *Theranostics* **2018,** *8*, 5012-5024.
35. Marbella, L. E.; Millstone, J. E., NMR techniques for noble metal nanoparticles. *Chem. Mater.* **2015,** *27*, 2721-2739.
36. Ruks, T.; Beuck, C.; Schaller, T.; Niemeyer, F.; Zähres, M.; Loza, K.; Heggen, M.; Hagemann, U.; Mayer, C.; Bayer, P., et al., Solution NMR spectroscopy with isotope-labelled cysteine ($^{13}C$, $^{15}N$) reveals the surface structure of L-cysteine-coated ultrasmall gold nanoparticles (1.8 nm). *Langmuir* **2019,** *35*, 767-778.
37. van der Meer, S. B.; Seiler, T.; Buchmann, C.; Partalidou, G.; Boden, S.; Loza, K.; Heggen, M.; Linders, J.; Prymak, O.; Hartmann, L., et al., Controlling the surface functionalization of ultrasmall gold nanoparticles by sequence-defined macromolecules. *Chem. Eur. J.* **2020**, https://doi.org/10.1002/chem.202003804.
38. Schrader, T.; Bitan, G.; Klärner, F. G., Molecular tweezers for lysine and arginine – powerful inhibitors of pathologic protein aggregation. *Chem. Commun.* **2016,** *52*, 11318-11334.
39. Trusch, F.; Kowski, K.; Bravo-Rodriguez, K.; Beuck, C.; Sowislok, A.; Wettig, B.; Matena, A.; Sanchez-Garcia, E.; Meyer, H.; Schrader, T., et al., Molecular tweezers target a protein–protein interface and thereby modulate complex formation. *Chem. Commun.* **2016,** *52*, 14141-14144.
40. Heid, C.; Sowislok, A.; Schaller, T.; Niemeyer, F.; Klärner, F. G.; Schrader, T., Molecular tweezers with additional recognition sites. *Chem. Eur. J.* **2018,** *24*, 11332-11343.
41. Fokkens, M.; Schrader, T.; Klärner, F. G., A molecular tweezer for lysine and arginine. *J. Am. Chem. Soc.* **2005,** *127*, 14415-14421.
42. Bier, D.; Rose, R.; Bravo-Rodriguez, K.; Bartel, M.; Ramirez-Anguita, J. M.; Dutt, S.; Wilch, C.; Klärner, F. G.; Sanchez-Garcia, E.; Schrader, T., et al., Molecular tweezers modulate 14-3-3 protein-protein interactions. *Nat. Chem.* **2013,** *5*, 234-239.
43. Kowalski, J. A.; Liu, K.; Kelly, J. W., NMR solution structure of the isolated Apo Pin1 WW domain: comparison to the x-ray crystal structures of Pin1. *Biopolymers* **2002,** *63*, 111-121.
44. Luh, L. M.; Hansel, R.; Lohr, F.; Kirchner, D. K.; Krauskopf, K.; Pitzius, S.; Schafer, B.; Tufar, P.; Corbeski, I.; Guntert, P., et al., Molecular crowding drives active Pin1 into nonspecific complexes with endogenous proteins prior to substrate recognition. *J. Am. Chem. Soc.* **2013,** *135*, 13796-13803.
45. Schelhorn, C.; Martin-Malpartida, P.; Sunol, D.; Macias, M. J., Structural Analysis of the Pin1-CPEB1 interaction and its potential role in CPEB1 degradation. *Sci. Rep.* **2015,** *5*, 14990.
46. Sekerina, E.; Rahfeld, J. U.; Muller, J.; Fanghanel, J.; Rascher, C.; Fischer, G.; Bayer, P., NMR solution structure of hPar14 reveals similarity to the peptidyl prolyl cis/trans isomerase domain of the mitotic regulator hPin1 but indicates a different functionality of the protein. *J. Mol. Biol.* **2000,** *301*, 1003-1017.
47. Wintjens, R.; Wieruszeski, J. M.; Drobecq, H.; Rousselot-Pailley, P.; Buée, L.; Lippens, G.; Landrieu, I., 1H NMR study on the binding of Pin1 Trp-Trp domain with phosphothreonine peptides. *J. Biol. Chem.* **2001,** *276*, 25150-25156.
48. Frassanito, M. A.; Saltarella, I.; Vinella, A.; Muzio, L. L.; Pannone, G.; Fumarulo, R.; Vacca, A.; Mariggiò, M. A., Survivin overexpression in head and neck squamous cell carcinomas as a new therapeutic target (Review). *Oncol. Rep.* **2019,** *41*, 2615-2624.

49. Martínez-García, D.; Manero-Rupérez, N.; Quesada, R.; Korrodi-Gregório, L.; Soto-Cerrato, V., Therapeutic strategies involving survivin inhibition in cancer. *Med. Res. Rev.* **2019,** *39*, 887-909.
50. Zafari, P.; Rafiei, A.; Esmaeili, S. A.; Moonesi, M.; Taghadosi, M., Survivin a pivotal antiapoptotic protein in rheumatoid arthritis. *J. Cell. Physiol.* **2019,** *234*, 21575-21587.
51. Rafatmanesh, A.; Behjati, M.; Mobasseri, N.; Sarvizadeh, M.; Mazoochi, T.; Karimian, M., The survivin molecule as a double-edged sword in cellular physiologic and pathologic conditions and its role as a potential biomarker and therapeutic target in cancer. *J. Cell. Physiol.* **2020,** *235*, 725-744.
52. Brust, M.; Fink, J.; Bethell, D.; Schiffrin, D. J.; Kiely, C., Synthesis and reactions of functionalised gold nanoparticles. *Chem. Commun.* **1995**, 1655-1656.
53. Häkkinen, H., The gold–sulfur interface at the nanoscale. *Nat. Chem.* **2012,** *4*, 443-455.
54. Hogeweg, A.; Sowislok, A.; Schrader, T.; Beuck, C., An NMR method to pinpoint supramolecular ligand binding to basic residues on proteins. *Angew. Chem. Int. Ed.* **2017,** *56*, 14758-14762.
55. Thust, A.; Barthel, J.; Tillmann, K., FEI Titan 80-300 TEM. *J. Large-scale Res. Fac.* **2016,** *2*, A41.
56. Altieri, A. S.; Hinton, D. P.; Byrd, R. A., Association of biomolecular systems via pulsed-field gradient NMR self-diffusion measurements. *J. Am. Chem. Soc.* **1995,** *117*, 7566-7567.
57. Stejskal, E. O.; Tanner, J. E., Spin diffusion measurements: Spin echoes in the presence of a time-dependent field gradient. *J. Chem. Phys.* **1965,** *42*, 288.
58. Esadze, A.; Zandarashvili, L.; Iwahara, J., Effective strategy to assign $^{1}H$-$^{15}N$ heteronuclear correlation NMR signals from lysine side-chain $NH_3^+$ groups of proteins at low temperature. *J. Biomol. NMR* **2014,** *60*, 23-27.
59. Iwahara, J.; Jung, Y. S.; Clore, G. M., Heteronuclear NMR spectroscopy for lysine NH(3) groups in proteins: unique effect of water exchange on (15)N transverse relaxation. *J. Am. Chem. Soc.* **2007,** *129*, 2971-2980.
60. Zandarashvili, L.; Esadze, A.; Iwahara, J., NMR studies on the dynamics of hydrogen bonds and ion pairs involving lysine side chains of proteins. *Adv. Protein Chem. Struct. Biol.* **2013,** *93*, 37-80.
61. Ayed, A.; Mulder, F. A.; Yi, G. S.; Lu, Y.; Kay, L. E.; Arrowsmith, C. H., Latent and active p53 are identical in conformation. *Nat. Struct. Biol.* **2001,** *8*, 756-760.
62. Mahl, D.; Diendorf, J.; Meyer-Zaika, W.; Epple, M., Possibilities and limitations of different analytical methods for the size determination of a bimodal dispersion of metallic nanoparticles. *Coll. Surf. A* **2011,** *377*, 386-392.
63. Yu, R.; Liz-Marzán, L. M.; García de Abajo, F. J., Universal analytical modeling of plasmonic nanoparticles. *Chem. Soc. Rev.* **2017,** *46*, 6710-6724.
64. Salorinne, K.; Malola, S.; Wong, O. A.; Rithner, C. D.; Chen, X.; Ackerson, C. J.; Häkkinen, H., Conformation and dynamics of the ligand shell of a water-soluble $Au_{102}$ nanoparticle. *Nat. Comm.* **2016,** *7*, 10401.
65. Akoka, S.; Barantin, L.; Trierweiler, M., Concentration measurement by proton NMR using the ERETIC method. *Anal. Chem.* **1999,** *71*, 2554-2557.
66. Mallon, M.; Dutt, S.; Schrader, T.; Crowley, P. B., Protein camouflage: Supramolecular anion recognition by Ubiquitin. *ChemBioChem* **2016,** *17*, 774-783.

**Graphical abstract**